LAWRENCE
LIVERMORE
NATIONAL
LABORATORY

UCRL-CONF-230974

On Tenth Order Central Spatial Schemes

B. Sjogreen, H. C. Yee

May 15, 2007

Fifth International Symposium on Turbulence and Shear Flow Phenomena
Munich, Germany
August 27, 2007 through August 29, 2007

Disclaimer

ON TENTH ORDER CENTRAL SPATIAL SCHEMES

Björn Sjögreen*
Center for Applied Scientific Computing,
Lawrence Livermore National Laboratory
Livermore, CA 94551, USA
sjogreen2@llnl.gov

H.C.Yee
NASA Ames Research Center,
Moffett Field, CA 94035, USA
hmcyee@mail.arc.nasa.gov

ABSTRACT

This paper explores the performance of the tenth-order central spatial scheme and derives the accompanying energy-norm stable summation-by-parts (SBP) boundary operators. The objective is to employ the resulting tenth-order spatial differencing with the stable SBP boundary operators as a base scheme in the framework of adaptive numerical dissipation control in high order multistep filter schemes of Yee et al. (1999), Yee and Sjögreen (2002, 2005, 2006, 2007), and Sjögreen and Yee (2004). These schemes were designed for multiscale turbulence flows including strong shock waves and combustion.

INTRODUCTION

The accuracy and stability of the overall high order central difference operators employing the traditional ways of implementing numerical boundary conditions by reducing the orders of the central scheme near the non-periodic boundary are greatly compromised. In the 80's and 90's, major effort was placed on the development of high order shock-capturing schemes and high order compact spatial schemes. Traditional high order central schemes were considered neither stable nor robust enough to be used in a more practical setting. In the work of Kriess and Scherer (1974, 1977), Strand (1994), Olsson (1995), Mattsson (2003), Svärd (2004) and references cited therein, high order finite difference operators with summation-by-parts (SBP) stable energy estimates were derived for the first derivative approximations for centered difference operator (for the interior grid points) of orders up to eight. The use of standard central spatial schemes thus regained its momentum in the mid and late 90's. The use of these SBP central schemes of order up to eight have been used with much success as the spatial base scheme in the adaptive numerical dissipation control multistep high order filter schemes of Yee and Sjögreen (1999,2002, 2005, 2006, 2007) and Sjögreen and Yee (2002, 2003, 2004). Test examples concentrated mainly on sixth-order or lower SBP central spatial base schemes. Improved accuracy over standard high order shock-capturing schemes was obtained for multiscale shock/turbulence interactions. From here on, the use of the phrase, e.g., "SBP central schemes of tenth-order" to mean the use of the tenth-order centered differencing interior scheme (for the interior grid points) with the accompanying stable SBP boundary operators that are usually much lower than the interior scheme.

In this work, the tenth-order central spatial differencing with stable SBP boundary operators are derived with numerical examples. The next section illustrates the performance of the tenth-order scheme for problems with periodic physical boundaries. The SBP boundary operators for the tenth-order centered differencing are derived with a 1-D shock/turbulence interaction example in the subsequent sections. 2-D and 3-D examples are in progress and will be reported in a forthcoming paper.

TEST CASES WITH PERIODIC BOUNDARY CONDITIONS

This section shows the performance of the tenth-order spatial scheme for several test cases with periodic boundary conditions. Note that in this case, SBP boundary operators are not needed.

The seven-point sixth-order accurate centered difference operator with an eighth-order numerical dissipation, is denoted by D06AD8. The eleven-point tenth-order accurate centered difference operator with twelfth-order numerical dissipation is denoted by D10AD12. Similarly, D08AD10 denotes the eighth-order centered difference operator tenth-order numerical dissipation. These operators are used for the spatial derivatives in the Euler equations. The classical fourth order accurate Runge-Kutta method is used for the time integration. In all of the examples, different time step sizes that are below the CFL limit were used. However, their results indicate no significant difference in the accuracy, indicating that the error of the spatial discretization dominates the temporal error.

The first example is the same isentropic vortex convection problem considered in Yee et al. (1999) and Sjogreen and Yee (2002). The computational domain is $[0, 18] \times [0, 18]$.

*Work performed under the auspices of the U.S. Department of Energy by University of California Lawrence Livermore National Laboratory under contract No. W-7405-Eng-48. UCRL-XXXX-XXXXXX

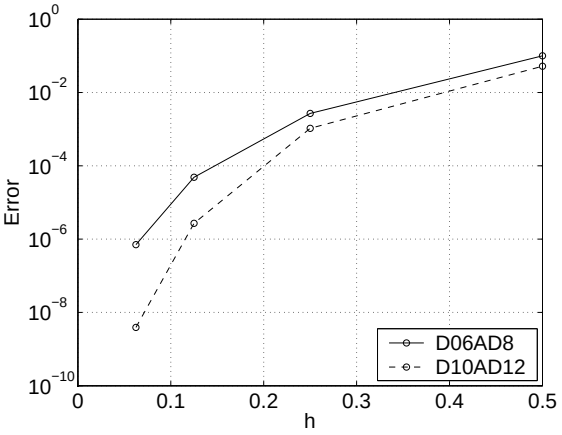

Figure 1: L^2 norm of the error in the density after the vortex has convected one period as function of the grid spacing, h. Sixth-order method (solid) and tenth-order method (dash).

The initial data is

$$\rho(0,x,y) = \left(1 - \frac{\beta^2(\gamma-1)}{8\gamma\pi^2} e^{1-r^2}\right)^{\frac{1}{\gamma-1}} \tag{1}$$

$$u(0,x,y) = u_\infty - \frac{\beta}{2\pi}(y-y_0)e^{(1-r^2)/2} \tag{2}$$

$$v(0,x,y) = v_\infty + \frac{\beta}{2\pi}(x-x_0)e^{(1-r^2)/2} \tag{3}$$

$$p(0,x,y) = \rho(0,x,y)^\gamma \tag{4}$$

where ρ is the density, u is the velocity in the x-direction, v is the velocity in the y-direction, and p is the pressure. γ is the ratio of specific heats. Here, $\gamma = 1.4$, $\beta = 5$, $u_\infty = 1$, and $v_\infty = 0$. $r^2 = (x-x_0)^2+(y-y_0)^2$, where the initial center of the vortex is $(x_0, y_0) = (9, 9)$. The boundary conditions are periodic in both directions. The exact solution consists of a translation of the initial data with the free stream velocity.

Fig. 1 displays the L^2 error in the density after one computational domain period of time integration with D06AD8 (solid line) and D10AD12 (dashed line) for four uniform grids with spacings $h = 0.5$, 0.25, 0.125, and 0.0625. We infer from Fig. 1 that the error of the 10th order method is always smaller than the error of the sixth-order method, but that the errors of both methods converge slower than the formal order of accuracy for the first two refinements. At the last refinement, the results are closer to the expected convergence rate. The error of the sixth-order method decreases by a factor 69, when we refine from $h = 0.125$ to $h = 0.0625$. The corresponding decrease of the error in the tenth-order method is a factor 692. The reduction of the error between the coarsest grids is slow because the computation is under resolved for h larger than 0.25. The highest significant frequencies are not resolved with any points per wavelength; points per wavelength results become meaningless. Computations without the added numerical dissipation are also stable. However, spurious oscillations due to nonlinear effect of the governing equations prevent the convection of the vortex to advance to a higher number of periods. See Sjögreen and Yee (2002) and Yee and Sjögreen (2002) for the behavior of central schemes with or without the AD8 and AD10 terms for longer time integration of this vortex convection problem.

In the second example we solve the 3-D Euler equations of gas dynamics with $\gamma = 5/3$ and with initial data

$$\rho(0,x,y,z) = 1 \tag{5}$$

$$u(0,x,y,z) = \sin(x)\cos(y)\cos(z) \tag{6}$$

$$v(0,x,y,z) = -\cos(x)\sin(y)\cos(z) \tag{7}$$

$$w(0,x,y,z) = 0 \tag{8}$$

$$p(0,x,y,z) = 100 + \frac{1}{16}((\cos(2z)+2)(\cos(2x)+\cos(2y)) - 2) \tag{9}$$

on the computational domain $[0, 2\pi] \times [0, 2\pi] \times [0, 2\pi]$. Here ρ is the density, p is the pressure, and u, v, w are the three velocity components. This is known as a Taylor-Green vortex. The computation stops at a total time equal to 10. The boundary conditions are periodic. The initial data is smooth, but the scales in the solution become smaller and smaller with time. The enstrophy (the square of the L^2 norm of the curl of the velocity) is often used as a measure of the content of small scales in the solution. For this problem, the added numerical dissipation AD8, AD10 and AD12 for the corresponding centered schemes are necessary for a stable time stepping.

In Fig. 2 we plot the enstrophy (normalized to 1 at time 0) as function of time for the sixth-order (dot), the eighth-order (dash) and the tenth-order (dash-dot) schemes, computed on a grid with $64 \times 64 \times 64$ grid points. We also plot the enstrophy obtained from the semi-analytical formulas given in Brachet et al. (1983), This "exact" solution is valid for times less than approximately 4 and we only plot it up to that time. The computed enstrophies agree well with the semi-analytical formula. For large times there is no accuracy, but Fig. 2 shows that the schemes with less numerical dissipation give higher enstrophy values. This means that the method with the highest order of accuracy has the largest small-scale content. The AD8, AD10 and AD12 dissipation coefficients used are 0.0001.

In Fig. 3, we show the same comparison as in Fig. 2, but for computations on a grid with $144 \times 144 \times 144$ points using the same numerical dissipation coefficient of 0.0001 (except for the sixth-order scheme). The maximum enstrophy now is higher (note different scaling) for all methods, reflecting the fact that higher frequencies can be supported on a finer grid. For the same dissipation coefficient, 0.0001, the sixth-order central scheme is convecting extremely slow of an unacceptable rate, thus a 10 times larger numerical dissipation coefficient, 0.001 was used for AD8.

The same computations using comparable dissipation coefficients for AD8, AD10 and AD12 are shown in Fig. 4 and Fig. 5/. That is the strengths of the numerical dissipation operators are set to be equivalent for all three methods. The solution of the tenth-order scheme appears to follow the semi-analytical solution closer. It is clear from Fig. 4 that the tenth-order method is better at supporting the small scales, because the enstrophy is higher for large times. In this case, the tenth-order central scheme is more accurate than its eighth-order and sixth-order counterparts.

Both the above examples show error reduction with the tenth-order accurate scheme for problems with periodic boundary conditions. In order to extend the tenth-order computations to problems with non-periodic boundaries, special stable boundary operators are needed. We are particularly interested in deriving energy stable SBP boundary operators for the tenth-order interior operator. One such derivation is presented next.

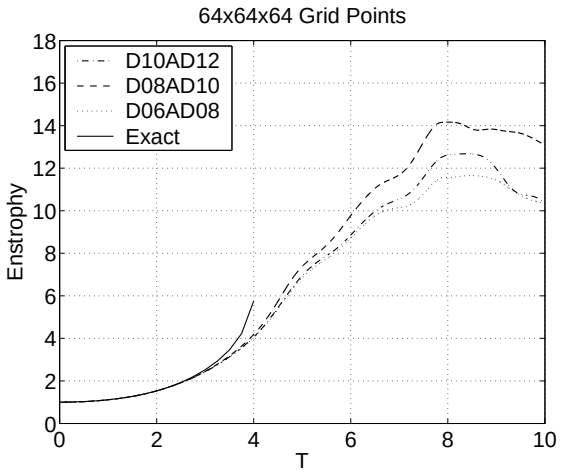

Figure 2: Enstrophy vs time for the Talyor-Green vortex. 64^3 grid points for dissipation coefficient of AD8, AD10 and AD12 equal to 0.0001. Sixth-order method (dot), eighth-order method (dash), tenth-order method (dash-dot), and semi-analytical (solid).

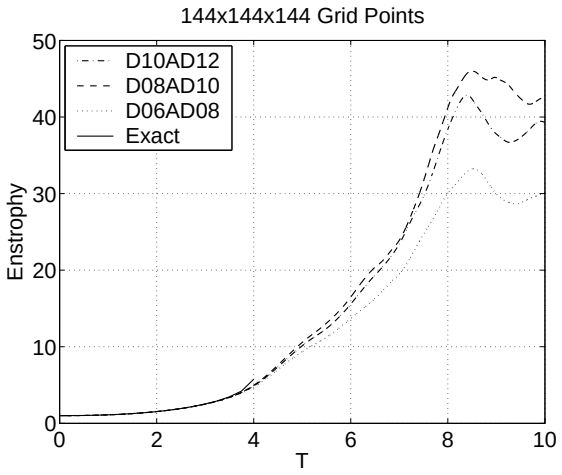

Figure 3: Enstrophy vs time for the Talyor-Green vortex. 144^3 grid points. Sixth-order method (dot), eighth-order method (dash), tenth-order method (dash-dot), and semi-analytical (solid).

SBP DIFFERENCE OPERATORS

Here, we follow Strand (1994) to determine boundary modification for tenth-order accurate interior approximations of d/dx. We consider a uniform grid x_j, $j = 1, 2, 3, \ldots$ with grid spacing $h = x_{j+1} - x_j$. The difference operator approximating $du(x_j)/dx$ is of the form

$$h\tilde{D}u_j = \begin{cases} \sum_{k=1}^{s} q_{j,k} u_k & j = 1, 2, \ldots, r \\ \sum_{k=-q}^{q} \alpha_k u_{j+k} & j = r+1, r+2, \ldots \end{cases}.$$

The interior approximation is defined by the coefficients α_k. The $2q$th order accurate interior approximation has $\alpha_{-k} = -\alpha_k$ and is used for $j > r$, where r is an arbitrary number $> q$. The boundary modified operator acts at the points $j = 1, \ldots, r$, and is defined by the coefficients $q_{j,k}$. The SBP boundary operators satisfy the identity

$$(u, Dv)_h = -(Du, v)_h - u_1 v_1$$

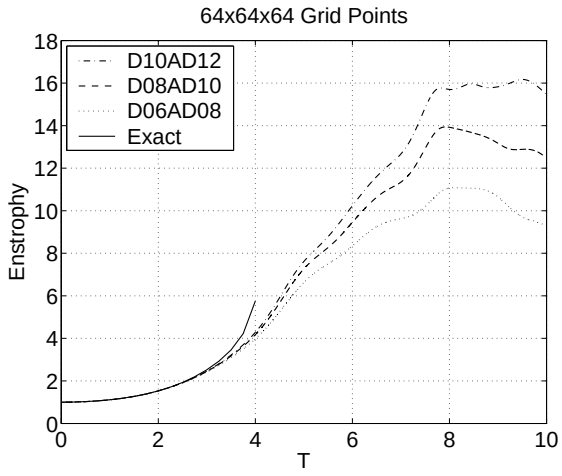

Figure 4: Enstrophy vs time for the Talyor-Green vortex. 64^3 grid points using relative dissipation coefficient strength. Sixth-order method with AD8 coeff. $= 0.0016$ (dot), Eighth-order method with AD10 coeff. $= 0.0004$ (dash), tenth-order method with AD12 coeff. $= 0.0001$ (dash-dot), and semi-analytical (solid).

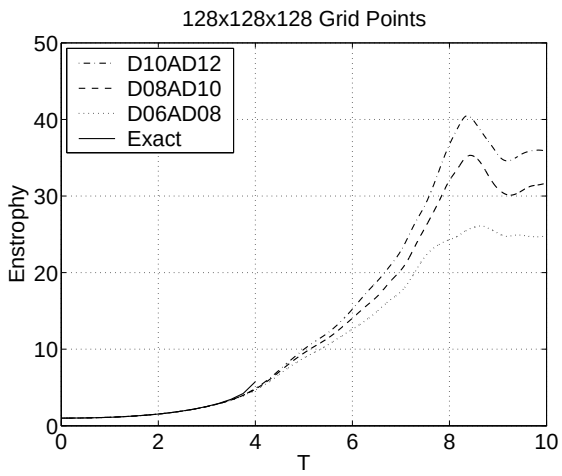

Figure 5: Enstrophy vs time for the Talyor-Green vortex. 64^3 grid points using relative dissipation coefficient strength. Sixth-order method with AD8 coeff. $= 0.0016$ (dot), Eighth-order method with AD10 coeff. $= 0.0004$ (dash), tenth-order method with AD12 coeff. $= 0.0001$ (dash-dot), and semi-analytical (solid).

for all grid functions u and v where $(u, v)_h$ is a discrete scalar product. This makes it possible to prove estimates for the difference approximation.

We write the difference operator on block matrix form as

$$h\tilde{D} = \begin{pmatrix} Q_1 & Q_2 \\ -C^T & D \end{pmatrix},$$

where $Q = (Q_1\ Q_2)$ is the matrix formed by the coefficients $q_{j,k}$. Q_1 is of size $r \times r$. C and D are determined by the interior discretization. When the order of accuracy is $2q$, D is of the form

$$D = diag(-\alpha_q, -\alpha_{q-1}, \ldots, -\alpha_1, 0, \alpha_1, \ldots, \alpha_q).$$

The matrix C holds the part of the interior discretization

that extends outside the first rows of D, i.e.,

$$-C^T = \begin{pmatrix} 0 & \dots & 0 & -\alpha_q & -\alpha_{q-1} & \dots & -\alpha_1 \\ 0 & \dots & 0 & 0 & -\alpha_q & \dots & -\alpha_2 \\ \dots & \dots & \dots & \dots & \dots & \dots & \dots \\ 0 & \dots & 0 & 0 & 0 & \dots & -\alpha_q \\ 0 & \dots & 0 & 0 & 0 & \dots & 0 \\ \dots & \dots & \dots & \dots & \dots & \dots & \dots \end{pmatrix}$$

Q_2 and C are of size $r \times (s-r)$. s can be considered arbitrarily large with the rows of Q_2 and C padded with zeros.

Taylor expansion gives the equations for pth order of accuracy at the boundary,

$$QE = F \tag{10}$$

where $(E)_{i,j} = (i-1)^{j-1}$ and $(F)_{i,j} = (j-1)(i-1)^{j-2}$ and where any occurrence of 0^0 is interpreted as 1. The sizes of E and F are $s \times (p+1)$ and $r \times (p+1)$ respectively. We partition E as $E = \begin{pmatrix} E_1 \\ E_2 \end{pmatrix}$ with E_1 of size $r \times (p+1)$ and write (10) as

$$Q_1 E_1 + Q_2 E_2 = F. \tag{11}$$

The summation by parts property is equivalent with

$$(u, \tilde{D}u)_H = -\frac{1}{2}u_1^2$$

where the weighted scalar product is given by $(u,v)_H = (u^I)^T H v^I + (u^{II})^T v^{II}$, for a positive definite $r \times r$ matrix H. We define $u^I = (u_1, \dots, u_r)$ and $u^{II} = (u_{r+1}, u_{r+2}, \dots)$. The summation by parts property is equivalent with

$$HQ_1 = B_1 + B_2 \tag{12}$$

$$HQ_2 = C \tag{13}$$

where B_1 is the matrix with $-1/2$ as (1,1) element and all other elements equal to zero. B_2 is an arbitrary anti-symmetric matrix. The summation by parts boundary operators are found by solving (11), (12), and (13) for Q_1, Q_2, and H.

To solve these equations, we multiply (11) by H and use (12) and (13) to substitute HQ_1 and HQ_2. This results in the equation

$$B_2 E_1 + B_1 E_1 + C E_2 = HF \tag{14}$$

for B_2. We multiply (14) by E_1^T and use the anti-symmetry $(E_1^T B_2 E_1)^T = -E_1^T B_2 E_1$ to obtain the solvability condition

$$F^T H E_1 + E_1^T H F = 2E_1^T B_1 E_1 + E_1^T C E_2 + E_2^T C^T E_1 \triangleq M, \tag{15}$$

which is a linear system of $(p+1)^2$ equations for the r^2 unknown elements of H. Note that M only depends on the interior discretization and on r. It was shown in Strand (1994) that (15) can be solved in the following cases

- p is odd, the interior discretization is $p+1$th order accurate, and $r = p+1$, i.e., the number of equations and unknowns are equal in (15). H is called a full norm.
- p is odd, the interior discretization is $p+1$th order accurate, $r = p+2$, and all elements, except the (1,1) element, on the first row of H are equal to zero. H is called a restricted full norm.
- H is diagonal, the interior discretization is $2p$th order accurate, and $r = 2p$. H is called a diagonal norm.

Table 1: Summary of known SBP operators.

Norm type	B-order p	# param.	Ref.
full	3	2	Strand (1994)
full	5	3	Mattson (2003)
full	7	4	Mattson (2003)
restricted	3	3	Strand (1994)
diagonal	1	0	Strand (1994)
diagonal	2	0	Strand (1994)
diagonal	3	1	Strand (1994)
diagonal	4	3	Strand (1994)

Note that the existence of a solution H is not enough; in order for H to be a norm, H has to be positive definite as well. It was shown in Strand (1994) that a positive definite H can be found if r is made sufficiently large, but there is no guarantee that optimal properties $r = p+1$, $r = p+2$, and $r = 2p$ (for the three above cases) can be satisfied with H positive definite.

Energy estimates for PDEs obtained in one space dimension with the full norm operator do not generalize to two space dimensions, because the full norms in the x- and y-directions do not, in general, commute. With the diagonal norm, these operators do commute and estimates can be carried over from one dimensional problems to multidimensional problems. However, our experience from practical computations is that the full norm operators also perform well in multi dimensions.

After having solved (15) for H, we insert H into (14) and solve for B_2. (14) is usually underdetermined and we obtain a solution that depends on a number of parameters. With H and B_2 known, (12) and (13) give $Q_1 = H^{-1}(B_1 + B_2)$ and $Q_2 = H^{-1}C$. The SBP boundary operator is determined. Table 1 summarizes a few known SBP operators. The second column shows the boundary order p and the third column displays the number of free parameters in the operator.

Olsson (1992) derived the same operators as Strand (1994). Mattson (2003) gave one operator, not the parametric dependency.

The freedom given by the undetermined parameters can be used, e.g., to determine an operator with a minimal spectral radius. This maximizes the time step if the operator is used in an explicit time stepping scheme.

SBP Operators with Tenth-Order Accuracy in the Interior

The tenth-order accurate centered finite difference operator has the coefficients

$$\alpha_1 = 5/6 \quad \alpha_2 = -5/21 \quad \alpha_3 = 5/84 \quad \alpha_4 = -5/504 \quad \alpha_5 = 1/1260. \tag{16}$$

We use this as the interior discretization and solve (15) for a diagonal norm with $p = 5, r = 10$." It turns out that the solution has negative elements, i.e., H is not positive definite. Similarly, solving for a diagonal norm SBP operator with $(p = 6, r = 12)$, $(p = 7, r = 14)$, and $(p = 8, r = 16)$ all give non-positive definite Hs. We use this as the interior discretization and solve (15) with $p = 5, r = 10$. It turns out that the solution has negative elements, i.e., H is not positive definite. Similarly, the pairs $(p = 6, r = 12)$, $(p = 7, r = 14)$,

and ($p = 8, r = 16$) all give non-positive definite H's. We conjecture that there are no diagonal norms as defined in Strand (1994) for $p > 4$.

Instead we take $p = 5$ and $r = 11$ to obtain an H that depends on one parameter. For a certain interval of the parameter, H is positive definite. We fix this parameter in the middle of the interval of positive definiteness to obtain the norm

$$H = diag(62715991/217728000, 10645069/6773760, 922613/6350400, 11862631/6350400, 678527/1036800, 21626453/36288000, 2887/1620, 678527/1814400, 130522139/101606400, 282939397/304819200, 64002913/63504000). \quad (17)$$

The SBP boundary operator, Q, thus obtained depends on 10 free parameters through the solution of (14). Setting random values of these parameters typically leads to an operator with a spectral radius of size 10^5, which is useless for any practical purpose. To overcome this problem, we used the `fminsearch` routine in Matlab to minimize the spectral radius of the difference operator with respect to the free parameters. The boundary operator obtained is presented in the Appendix. It has spectral radius 50, which is 20 times larger than the size of the interior operator, but it is small enough to enable some preliminary computations. The minimization problem is extremely ill-conditioned, and we have probably not reached the global minimum. This is a topic of continued investigation.

TEST CASE WITH NON-PERIODIC BOUNDARIES

The first test case is the 1-D compressible inviscid shock-turbulence interaction problem with initial data consisting of a shock propagating into an oscillatory density. The initial data is given by

$$(\rho_L,\ u_L,\ p_L) = (3.857143,\ 2.629369,\ 10.33333) \quad (18)$$

to the left of a shock located at $x = -4$, and

$$(\rho_R,\ u_R,\ p_R) = (1 + 0.2\sin(5x),\ 0,\ 1) \quad (19)$$

to the right of the shock. The problem is solved on the domain $[0, 5]$ with the boundary modified operator applied at all boundary points.

Fig. 6 shows the solution computed with the tenth-order spatial base scheme together with a nonlinear shock-capturing filter obtained as the dissipative portion of a fifth-order WENO scheme (Yee and Sjögreen, 1999, 2002, 2006). The computation used a uniform grid with 400 points. The solution is plotted in red and the solid black line is the reference solution by the standard fifth-order WENO scheme using 4000 grid points. The accuracy is almost indistinguishable from the SBP sixth-order and SBP eighth-order centered schemes computations. One major shortcoming of the SBP tenth-order scheme is that it has a very restricted CFL limit. It is an order of magnitude lower than its sixth-order and eighth-order counterparts. The present SBP boundary operators for the tenth-order central interior scheme is also used to simulate many 2-D and 3-D multiscale problems containing strong shock waves. Results indicated that there is no dramatic gain in accuracy among sixth-order, eighth-order and tenth-order central base scheme under the framework of our high order filter approach. Perhaps an improved filter strategy is needed for this type of multiscale

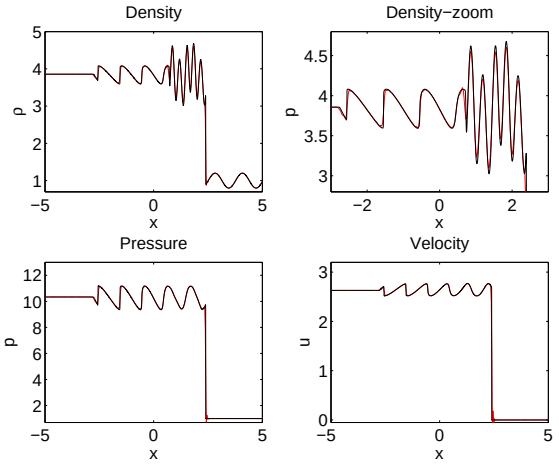

Figure 6: One dimensional shock-turbulence problem. Solution at time 1.6 computed by the new tenth-order SBP scheme with a fifth-order WENO based nonlinear filter (Yee and Sjögreen (2006)). Computed solution (red) and reference solution (black).

physics. The results will be reported in detail in a future publication.

SUMMARY

For coarse grid with periodic boundary conditions, the tenth-order central differencing is more accurate than lower order schemes. For the non-periodic boundary case, however, the CFL limit of the tenth-order scheme is an order of magnitude lower than the sixth-order and eighth-order counterparts. We have presented a fifth-order SBP boundary modification for the tenth-order interior central scheme. However, increasing the interior accuracy higher than eighth-order in the derivation of SBP operators lead to new difficulties. First it is non-trivial to make the norm matrices computed by the standard procedures positive definite. Second, the computed boundary operators usually have very large spectral radius. In the very high order case, both the norm matrices and the boundary operators depend on a large number of free parameters. In order to derive useful very high order summation by parts operators, it is necessary to use advanced optimization methods to select these parameters.

REFERENCES

Brachet, M.E., Meiron, D.I., Orszag, S.A., Nickel, B.G., and Morf, R.H., 1983, "Small-Scale Structure of the Taylor-Green Vortex", *J. Fluid Mech.*, Vol. 130, pp. 411–452.

Kriess, H.-O. and Scherer, G., 1974, "Finite Element and Finite Difference Methods for Hyperbolic Partial Differential Equations", *Partial Differential Equations*, Academic Press, Inc.

Kriess, H.-O. and Schere, G., 1977, "On the Existence of Energy Estimates for Difference Approximations for Hyperbolic Systems", Technical Report, Department of Scientific Computing, Uppsala University.

Mattson, K., 2003, "Summation-by-Parts Operators for High Order Finite Difference Methods", Ph.D. Thesis, Uppsala University, Information Technology, Department of Scientific Computing.

Olsson, P., 1992, "High-Order Difference Methods and

Dataparallel Implementation" Ph.D. Thesis, Uppsala University, Department of Scientific Computing.

Olsson, P., 1995, "Summation by Parts, Projections, and Stability. I", *Math. Comp.*, Vol. 64, pp. 1035–1065.

Strand, B., 1994, "Summation by Parts for Finite Difference Approximations for d/dx", *J. Comput. Phys.*, Vol. 110, pp. 47–67.

Sjögreen, B., and Yee, H.C., 2002, "Analysis of High Order Difference Methods for Multiscale Complex Compressible Flow", In *Proceedings of the HYP2002 conference*, Pasadena, CA, March 25-29.

Sjögreen, B., and Yee, H.C., 2003, "Grid Convergence of High Order Methods for Multiscale Complex Unsteady Viscous Compressible Flows", *J. Comput. Phys.*, Vol. 185, pp. 1–26.

Sjögreen, B., and Yee, H.C., 2004, "Multiresolution Wavelet Based Adaptive Numerical Dissipation Control for Shock-Turbulence Computation", *J. Sci. Comp.*, Vol. 20, pp. 211–255.

Yee, H.C., Sandham, N.D., Djomehri, M.J., 1999, "Low Dissipative High Order Shock-Capturing Methods Using Characteristic-Based Filters", *J. Comput. Phys.*, Vol. 110, pp. 47–67.

Yee, H.C., and Sjögreen, B., 2002, "Designing Adaptive Low Dissipative High Order Schemes for Long-Time Integrations", In *Turbulent Flow Computation*, Drikakis, D., and Geurts, B., ed., Kluwer Academic Publisher.

Yee, H.C., and Sjögreen, B., 2006, "Nonlinear Filtering and Limiting in High Order Methods for Ideal and Non-ideal MHD", *J. Sci. Comp.*, Vol. 27, pp. 507–521.

Yee, H.C., and Sjögreen, B., 2006, "Efficient Low Dissipative High Order Scheme for Multiscale MHD Flows, II: Minimization of Div(B) Numerical Error", RIACS Technical Report TR03.10, July, 2003, NASA Ames Research Center; also, J. Scient. Computing, (2005) DOI: 10.1007/s10915-005-9004-5, Vol. 29, pp. 115-164.

Yee, H.C., and Sjögreen, B., 2007, "Development of Low Dissipative High Order Filter Schemes for Multiscale Navier-Stokes/MHD Systems", Proceedings of the CalSpace/UCR ASTRONUM Conference, Palm Springs, CA, March 27-30, 2006. Expanded version to appear in J. Comput. Physics, 2007, http://dx.doi.org/10.1016/j.jcp.2007.01.012.

APPENDIX

Here, we give the optimized boundary operator matrix Q for SBP diagonal norm operator with $p =$ and $r = 11$. The matrix has size 11×16. The first six columns are

−1.735825	0.770205	5.598258	−5.303959	−5.536114	8.779473
−0.141173	0.000000	−2.878976	4.617511	1.976732	−5.979838
−11.099373	31.141411	0.000000	−66.660594	24.507405	76.519010
0.817870	−3.884603	5.184510	0.000000	−4.617298	−2.222004
2.436671	−4.746727	−5.440561	13.179402	0.000000	3.250455
−4.243363	15.768336	−18.653725	6.964703	−3.569390	0.000000
0.032496	−0.934761	4.439107	−8.991291	9.017526	−4.486641
0.665259	−3.113476	4.933463	−1.255448	−5.426069	7.335731
1.219606	−3.744699	−0.311858	13.619471	−18.761465	8.494855
−1.663525	5.798644	−2.675419	−13.658515	22.817263	−11.670627
0.408393	−1.510655	1.024657	2.833466	−5.397210	2.924868

columns seven to 11 are

−0.201045	−0.863696	−5.438996	5.360636	−1.428936	0.000000
1.060019	0.740902	3.060986	−3.424987	0.968825	0.000000
−54.451379	−12.698941	2.757407	17.093239	−7.108185	0.000000
8.577760	0.251335	−9.365768	6.786950	−1.528751	0.000000
−24.555401	3.100611	36.826269	−32.362533	8.311814	0.000000
13.416241	−4.603151	−18.310359	18.177034	−4.946326	0.000000
0.000000	0.908621	0.088411	−0.060118	−0.013795	0.000445
−4.329925	0.000000	1.909337	−0.954379	0.259912	−0.026528
−0.122652	−0.555845	0.000000	−0.049806	0.173160	0.046337
0.115421	0.384507	0.068928	0.000000	0.685535	−0.256507
0.024392	−0.096441	−0.220705	−0.631367	0.000000	0.826837

and columns 12 to 16 are

0.000000	0.000000	0.000000	0.000000	0.000000
0.000000	0.000000	0.000000	0.000000	0.000000
0.000000	0.000000	0.000000	0.000000	0.000000
0.000000	0.000000	0.000000	0.000000	0.000000
0.000000	0.000000	0.000000	0.000000	0.000000
0.000000	0.000000	0.000000	0.000000	0.000000
0.000445	0.000000	0.000000	0.000000	0.000000
−0.026528	0.002122	0.000000	0.000000	0.000000
0.046337	−0.007723	0.000618	0.000000	0.000000
−0.256507	0.064127	−0.010688	0.000855	0.000000
0.826837	−0.236239	0.059060	−0.009843	0.000787